Geo-Mar Lett (2003) 23: 351–358
DOI 10.1007/s00367-003-0141-2

ORIGINAL

Henrik Svensen · Sverre Planke · Bjørn Jamtveit
Tom Pedersen

Seep carbonate formation controlled by hydrothermal vent complexes: a case study from the Vøring Basin, the Norwegian Sea

Received: 18 February 2003 / Accepted: 25 August 2003 / Published online: 10 October 2003

Abstract Several hundred hydrothermal vent complexes were formed in the Vøring Basin as a consequence of magmatic sill emplacement in the late Palaeocene. The 6607/12-1 exploration well was drilled through a 220-m-thick sequence of Eocene–Miocene diatomites with carbonate nodules above the apex of one of these vent complexes. Analysed calcites and dolomites from this interval have isotopic signatures typical for methane seep carbonates, with low $\delta^{13}C$ signatures of −28 to −54‰ PDB. The data suggest that the vent complex acted as a fluid migration pathway for about 50×10^6 years after its formation, leading to near-surface microbial activity and seep carbonate formation.

Introduction

Seeps are fluid and gas leakage from a surface vent, and are documented from continental and marine systems around the world (see Hovland and Judd 1988, and Aharon 1994 for reviews). The vents are commonly inhabited by micro- and macro-organisms which utilize energy from the seep fluids. Fluid–microbial interactions may induce precipitation of minerals which include carbonates with distinct isotopic signatures. These deposits provide a record of formation conditions. Carbonates are actively forming today in numerous seep locations (e.g. Hovland et al. 1987; Roberts and Aharon 1994; Adshead 1996; Peckmann et al. 2001; Greinert et al. 2001). Their ancient analogues in the geological record (e.g. Gaillard et al. 1992; Aiello et al. 2001; Campbell et al. 2002) are important scientific targets for understanding more about the biological and physical processes operating at seeps.

Active seeps have been discovered in a wide range of geological environments which include "stable" sedimentary basins with leaking petroleum reservoirs (e.g. the North Sea, the Gulf of Mexico), and pierced sedimentary basins in tectonically active areas with thick accumulations of overpressured clay-rich sediments (e.g. accretion settings in the Mediterranean Ocean and back-arc settings in the South Caspian Basin; Jakubov et al. 1971; Hovland et al. 1987; Robertson et al. 1996). Commonly, the fluids expelled at seep sites represent pore waters, oil and hydrocarbon gases (dominantly methane). These fluids are commonly expelled together with sediments in mud volcanoes (e.g. Jakubov et al. 1971; Higgins and Saunders 1974; Ritger et al. 1987; Le Pichon et al. 1990; Cita et al. 1995; Robertson et al. 1996; Dia et al. 1999; Milkov 2000; Kopf and Behrmann 2000).

This paper discusses a setting for fluid seeps which has previously received little attention: *volcanic sedimentary basins*, which are characterized by the presence of extensive magmatic intrusive complexes. We have identified >700 hydrothermal vent complexes on seismic reflection data in the Møre and Vøring basins offshore mid-Norway (Fig. 1). They are typically expressed as vertical zones of disturbed seismic data, extending from deeper, high-amplitude reflections (sills) to the palaeosurface. At the palaeosurface, the upper part of the hydrothermal vent complex is usually manifested as an eye-structure representing either a crater or a mound (see Figs. 2 and 3). The hydrothermal vent complexes were formed by phreatic eruptions subsequent to emplacement of magmatic sills in the late Palaeocene (Jamtveit et al. 2003). These systems are short-lived (on the scale of 10–100s of years), are gas-dominated, and are associated with sediment volcanism (Jamtveit et al. 2003). As a result, hydrothermal vent complexes

H. Svensen (✉) · S. Planke · B. Jamtveit
Physics of Geological Processes (PGP), University of Oslo,
P.O. Box 1048 Blindern, 0316 Oslo, Norway
E-mail: hsvensen@geo.uio.no

S. Planke
Volcanic Basin Petroleum Research (VBPR),
Oslo Research Park, 0349 Oslo, Norway

T. Pedersen
Institute for Energy Technology (IFE),
P.O. Box 40, 2027 Kjeller, Norway

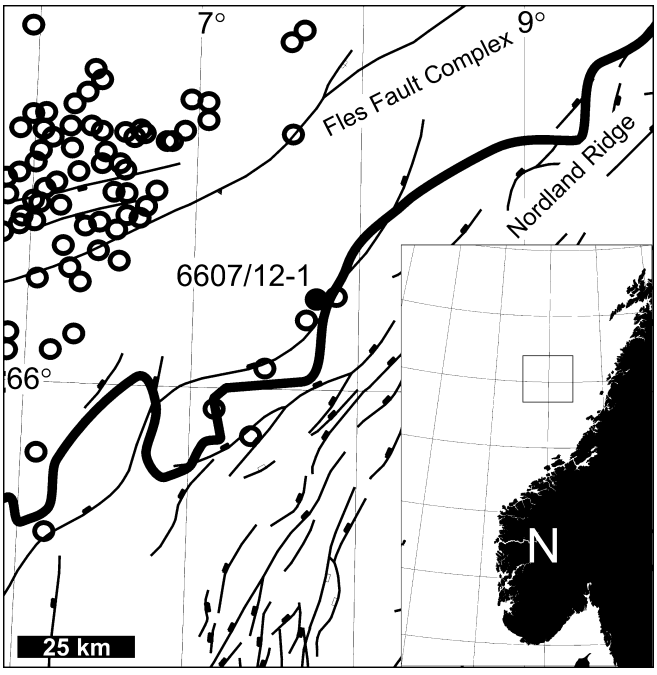

Fig. 1 Interpreted hydrothermal vent complexes (*circles*) in the eastern part of the Vøring Basin. The *thick line* marks the eastern limit of sill complexes in the area, *thin lines* mark faults. Structures from Blystad et al. (1995)

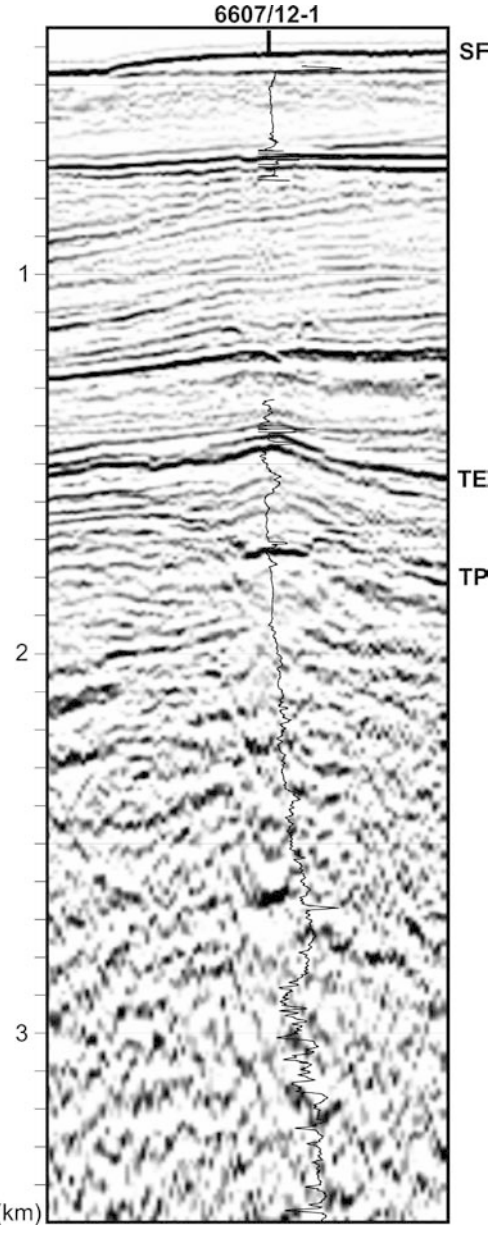

Fig. 2 Depth-converted seismic data of the 6607/12-1 hydrothermal vent complex. The wireline velocity log is shown for reference. *SF* Seafloor, *TE* top Eocene, *TP* top Palaeocene

are not commonly associated with significant mineral deposition.

The hydrocarbon exploration well 6607/12-1 in the Vøring Basin was drilled through the centre of a hydrothermal vent complex in 1986 and it provides a unique opportunity to study the geological structure and development of this complex. A project including sampling (~140 samples), biostratigraphy, seismic interpretations, petrography, and geochemistry of the well was completed in 2002. One of the aims of the study was to determine the nature of disturbed seismic reflectors both below and above eye structures which are commonly observed associated with hydrothermal vent complexes in the Vøring Basin. Furthermore, we aimed to test if these reflectors could be related to seep deposits. This contribution focus on the petrography and geochemistry of carbonates overlying the hydrothermal vent complex, and documents how this complex may have influenced long-term fluid migration and seeps in the basin.

The 6607/12-1 hydrothermal vent complex

The 6607/12-1 borehole was drilled to 3,521-m depth in 390-m water depth in 1986 (Figs. 1, 2 and 3). The 1,409–1,426 m interval was cored, with a recovery of 8.6 m. The well was subsequently plugged and abandoned as a dry hole.

The well is located at the crest of a regional dome of Palaeogene strata, in the centre of a hydrothermal vent complex. The vent complex is characterized by a 2-km-wide, eye-shaped upper part at the top Palaeocene level, above a zone of disrupted seismic data connecting the upper part of the vent complex with the termination of a high-amplitude seismic event at 5.0 s twt. This event is regionally interpreted as a sill intrusion. The strata above the vent complex form a mound up to the Top Mound horizon (Figs. 2 and 3).

The well penetrated 1,000 m of Recent to Plio/Pleistocene glacial clay and sand/gravel deposits, Eocene to upper Palaeocene diatomite ooze and claystone, and Cretaceous claystone and shales (Blunck and Blanchet 1986). Two main unconformities are recognized, a Miocene to Eocene unconformity at 1,400 m and an upper Palaeocene to Maastrichtian unconformity at

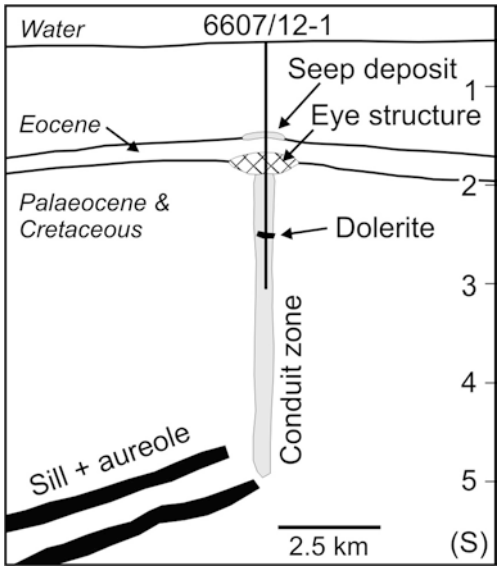

Fig. 3 Interpretation of sill geometry and the hydrothermal vent complex drilled in the 6607/12-1 borehole based on seismic data. A vertical zone of disturbed seismic data is interpreted as a conduit zone. The eye-shaped structure represents the upper part of the complex, probably formed by filling of an explosion crater. Similar relationships between sills, conduit zone, and palaeosurface deposits are observed in most of the >700 hydrothermal vent complexes from the Vøring and Møre basins

1,770 m. Both unconformities are correlated with seismic events which have been mapped regionally. The Eocene–Pliocene diatomite and claystone in the well contain stringers and layers of carbonates (calcite and dolomite). Carbonate is more abundant between 1,370 and 1,500 m than elsewhere in the stratigraphy, and correlates with strong seismic reflections and physical property changes recorded on wireline logs (Figs. 2 and 4).

Materials and methods

In all, 139 samples have been collected and analysed from the cored interval and from the cuttings of the well. Here we describe the results from carbonate petrographic and geochemical analyses from 30 samples in the 1,300–1,700 m interval. Stable isotopes of C and O were analysed from core samples, and from handpicked fractions from the cuttings. Stable isotope values are given for both calcite and dolomite in samples where they occur together. All samples for isotope analyses were initially analysed for mineralogy by XRD. Due to a limited amount of carbonate grains in the cuttings, the XRD analyses are in many cases the only information available on the carbonate composition (i.e. when no thin sections could be made). The handpicked fractions of carbonates from the cuttings were sorted according to appearance (texture, grain size, colour).

Stable isotope analyses of calcite and dolomite were conducted at the Institute of Energy Technology (IFE),

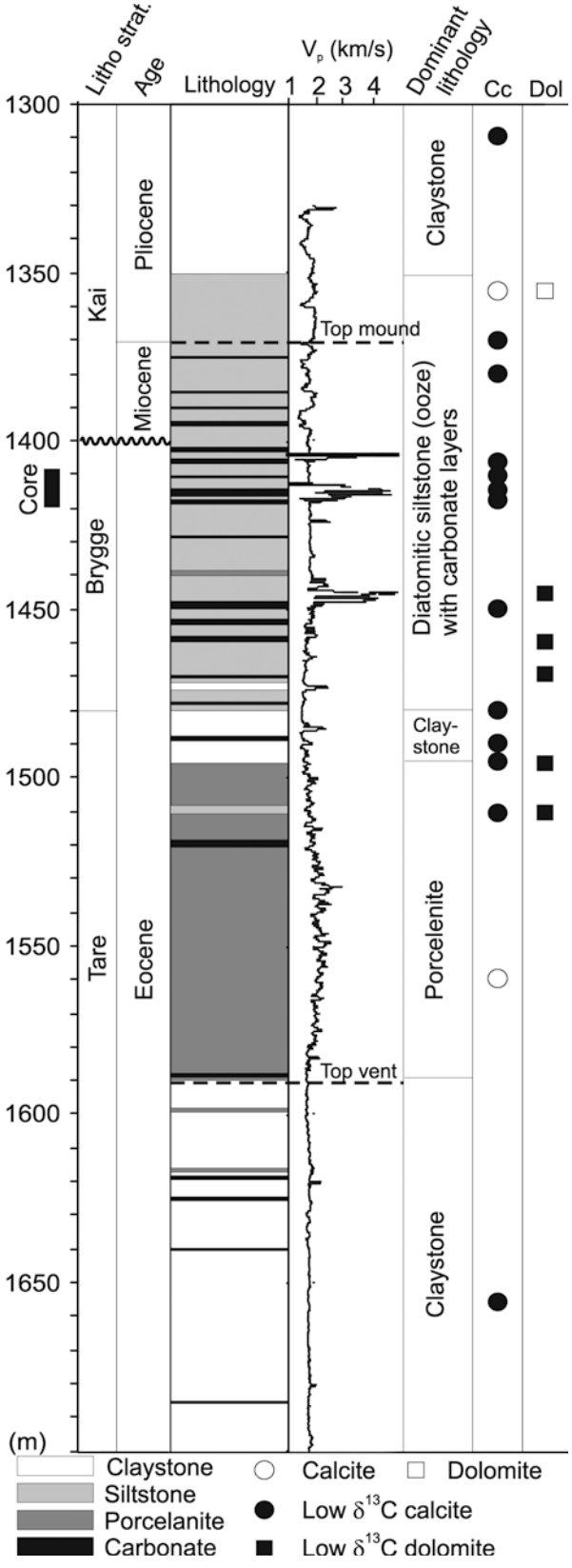

Fig. 4 Composite log of the 1,300–1,700 m interval from 6607/12-1. The stratigraphy is based upon the new biostratigraphy, our study of the cuttings, and Blunck and Blanchet (1986). Calcite is found in the core and the cuttings, mostly between 1,350 and 1,520 m

Norway. Organic material was removed prior to carbonate stable isotope analysis by vacuum heating the samples in a furnace for 4 h at 400 °C. The carbonates were reacted with H_3PO_4 under vacuum. Calcite was reacted for 2 h at 25.0 °C, whereas dolomite was reacted at 25.0 °C for 6 days. The released CO_2 was cryogenically purified and transferred to a Finnigan MAT 251 isotope ratio mass spectrometer (IRMS) with dual inlet and triple collector, for determination of $\delta^{13}C$ and $\delta^{18}O$. The precision for $\delta^{13}C$ is 0.1‰ and for $\delta^{18}O$ it is 0.2‰, and the dolomite $\delta^{18}O$ was corrected for phosphoric acid fractionation.

Cathodoluminescence on thin sections of carbonates was studied using a Cambridge Image Technology Cathodoluminescence CL820 MK4, at the Department of Geology, University of Oslo.

Results

Carbonate petrography and geochemistry

The limestone layers in the core are massive, with no apparent layering. Curved upper and lower surfaces indicate that they represent concretions, not continuous layers. Limestone is present in two horizons (< 10 cm thick) in the upper part of the core (1,409–1,414 m), whereas limestone comprises about 50% of the stratigraphy in the lower half of the core. The most prominent feature of the limestones is numerous small (< 0.5 cm), circular calcite nodules. The nodules occur throughout the limestones but are most easily seen along the upper and lower terminations of the layers (Fig. 5). The nodules comprise radial calcite crystals with undulating extinctions under crossed polars in the microscope, and are concentrically zoned when studied by cathodoluminescence. The zonation is due to the presence of Mn in the calcite, which has been verified by microprobe analyses (Svensen et al., unpublished data).

Although the nodules bear some resemblance to ooides, their origin is not related to reworking or ooid formation. The carbonate cements the diatomite (Fig. 6A–F), and thus precipitates within the porosity of the diatomite. Comparable carbonate textures are reported from Eocene diatomites in the Bering Sea (Hein et al. 1979), and nodular carbonates precipitated from seeps are known to form early diagenetic concretions (e.g. Raisewell 1987; Ritger et al. 1987; Aloisi et al. 2000). Vertical and sub-vertical calcite veins and breccias locally form branching networks in the limestone, and in some parts of the interbedded siltstone. The calcite is in textural equilibrium with pyrite, and pyrite is commonly present within microfossils (Fig. 6F). Compositionally, the carbonates in the core are calcites and Mg-calcites (Svensen et al., unpublished data).

The stable isotope (C and O) data on calcite show a high variation in isotopic compositions (Table 1), both with respect to $\delta^{13}C$ (from −54.1 to −1.1‰ PDB) and $\delta^{18}O$ (−6.6 to 5.8‰ PDB), and fall in two distinct groups (Fig. 7). Group I carbonates are represented by three analyses (two calcites and one dolomite) with $\delta^{13}C$ values between −1.1 and −9.0‰, and $\delta^{18}O$ values between −4.0 and −6.6‰. Group II carbonates (dolomite and calcite) have $\delta^{13}C$ values between −28.4 and −54.1‰, and $\delta^{18}O$ values between −2.0 and 5.8‰. Isotopically light carbon (i.e. group II carbonate) is present in 27 of the 30 analysed samples.

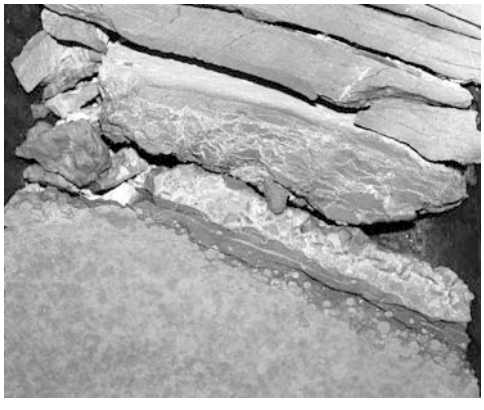

Fig. 5 Photograph of the core showing a limestone layer with calcite nodules (*bottom*), a calcite cemented breccia with clasts of diatomite ooze (*middle*), and diatomite ooze (*top*)

Discussion

The majority of the carbonates present in the strata above the hydrothermal vent complex (i.e. group II carbonates) have very depleted $\delta^{13}C$ values, down to −54‰ (Fig. 7). The isotopically light carbon in these carbonates indicates that the carbon is methanogenic (formed from oxidation of CH_4; e.g. Higgins and Quale 1970; Irwin et al. 1977; Reeburgh 1980; Ritger et al. 1987; Paull et al. 1992; Bohrmann et al. 1998; Stakes et al. 1999; Elvert et al. 2001; Greinert et al. 2001). The low $\delta^{13}C$ calcite is in textural equilibrium with pyrite, indicating that the precipitation was induced by anaerobe methane oxidation coupled with sulphate reduction (e.g. Kohn et al. 1998; Stakes et al. 1999; Hinrichs et al. 1999; Boetius et al. 2000; Peckmann et al. 2001, and references above). That pyrite is present within the microfossils may be explained by microfossils providing space, nutrients, and nucleation sites for pyrite growth (Kohn et al. 1998). The radial crystals in the calcite nodules from the group II carbonates may have originated as aragonite, and recrystallized to calcite during diagenesis. This is supported from a textural point of view when compared to modern seep carbonate deposits (e.g. Ritger et al. 1987; Hovland et al. 1987; Bohrmann et al. 1998; Aloisi et al. 2000).

The range in $\delta^{13}C$ of the bulk of the analysed group II carbonates (−28 to −40‰) indicates that the methane was either thermogenic or biogenic (cf. Suess and Whiticar 1989; Stakes et al. 1999). Methane of thermogenic origin usually has $\delta^{13}C$ between −30 and

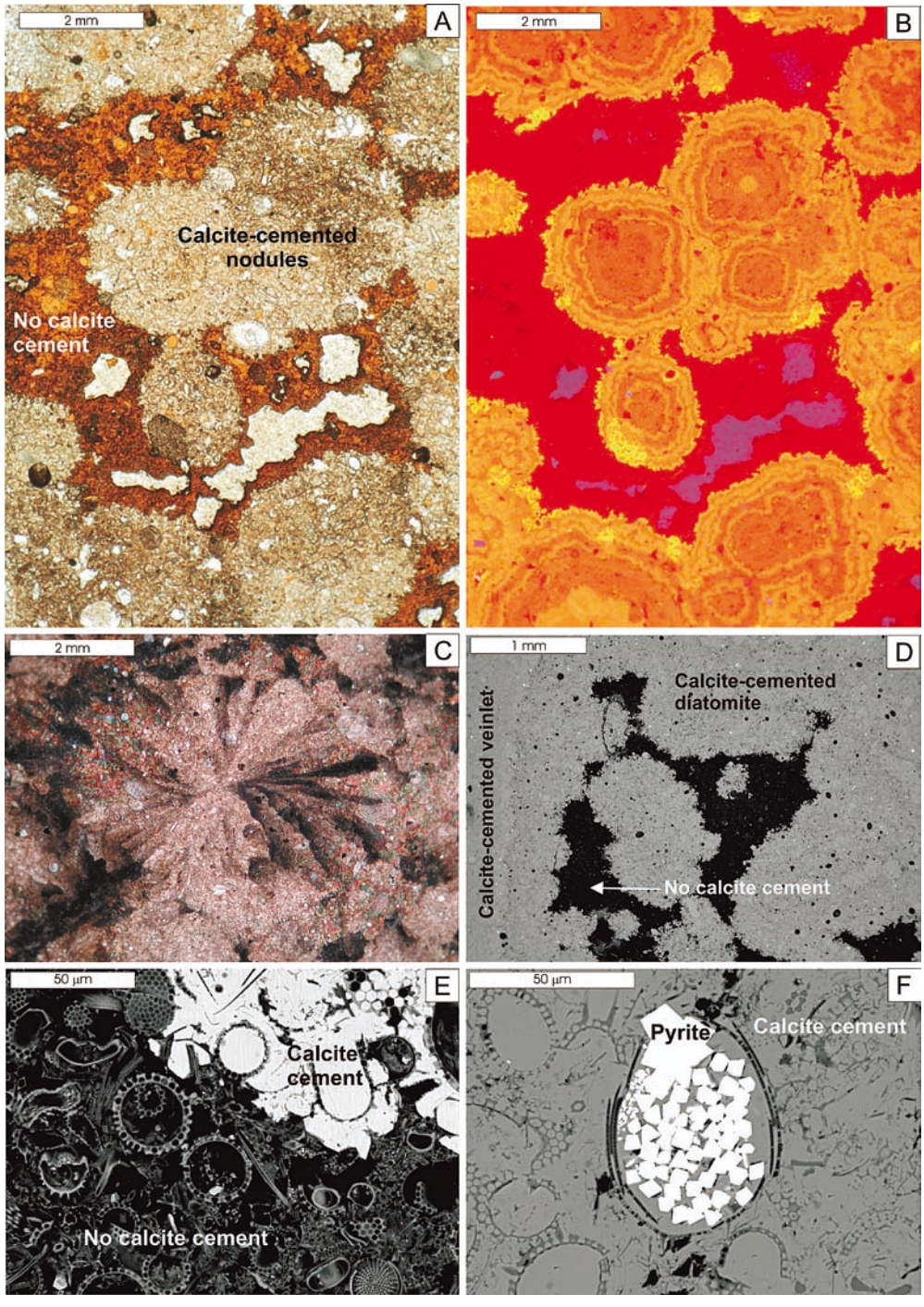

Fig. 6A–F Thin sections from the limestone in the core show the presence of calcite nodules (in transmitted light) cementing the diatomite ooze (**A**), with internal concentric chemical variations, as seen under luminescence (**B**). The nodules comprise radial crystals with typical undulating extinctions under crossed polars, optical microscope (**C**). SEM backscatter images (**D**–**F**) show that the calcite partly cements the diatomite (**D**), with a sharp transition between the calcite nodules and the rest of the diatomite ooze (**E**). Pyrite is abundant in the limestone, often as framboidal pyrite, or as clusters of small crystals filling microfossils (**F**)

−50‰, whereas biogenic methane is more fractionated (< −65‰; cf. Vinigradov and Galimov 1970; Irwin et al. 1977; Brooks et al. 1984; Whiticar et al. 1985; Ritger et al. 1987; Stakes et al. 1999). The lowest of the group II values (< −40‰) suggests a biogenic origin. The group I carbonates with $\delta^{13}C$ ratios between −9 and −1‰ are probably derived from seawater bicarbonate with a component of CO_2 from oxidized organic material, which commonly have $\delta^{13}C$ values around −20‰ (e.g. Irwin et al. 1977; Ritger et al. 1987).

The bimodal distribution of carbonate in the $\delta^{13}C$–$\delta^{18}O$ system (Fig. 7) has also been reported by other studies of seep carbonates, including the association of isotopically light $\delta^{13}C$ with isotopically heavier $\delta^{18}O$ (e.g. Ritger et al. 1987; Paull et al. 1992; Stakes et al. 1999; Aloisi et al. 2000). The presence of isotopically heavy carbonate ($\delta^{18}O$ values > 6‰) from a range of seep localities has been attributed to precipitation from $\delta^{18}O$-enriched fluids rather than being a temperature effect, where destabilization of gas hydrates is a likely

Table 1 Stable isotope analyses of carbonate from 6607/12-1 (all values are relative to PDB)

Sample	Depth (m)	Type	Lithology	Calcite		Dolomite	
				$\delta^{13}C$	$\delta^{18}O$	$\delta^{13}C$	$\delta^{18}O$
HS 76	1,310	Fragments	Pliocene	−45.9	5.1	−45.7	−1.5
HS76	1,310	Fragments	Pliocene	−45.9	5.1	−45.7	3.6
HS 12	1,355	Fragments	Pliocene	−9.0	−4.8	−5.3	−6.6
HS 13	1,370	Fragments	Miocene	−54.1	5.8		
HS 14	1,385	Fragments	Miocene	−33.6	2.9	−35.8	−1.5
HS 113	1,407	Fragments	Mound	−39.1	0.0		
HS 113	1,407	Fragments	Mound	−39.1	0.0		
HS 1	1,410.4	Core/limestone	Mound	−37.8	−0.7		
HS 3	1,411.1	Core/breccia	Mound	−37.4	−0.9		
HS 5	1,414.1	Core/breccia	Mound	−38.6	2.6		
HS 7	1,414.9	Core/limestone	Mound	−39.8	−0.7		
HS 9	1,415.7	Core/limestone	Mound	−39.5	−0.5		
HS 10	1,416.1	Core/limestone	Mound	−38.7	1.5		
HS 152	1,417.17	Core/limestone	Mound	−39.3	0.2		
HS 153	1,417.38	Core/limestone	Mound	−29.7	0.1		
HS 11	1,417.4	Core/limestone	Mound	−38.7	2.3		
HS 150	1,417.47	Core/limestone	Mound	−37.2	1.7		
HS 19	1,445	Fragments	Mound	−39.6	−0.2		
HS 20	1,450	Fragments	Mound			−33.8	−1.5
HS 20	1,450	Fragments	Mound	−38.6	0.7	−33.8	−1.5
HS 112	1,460	Fragments	Mound			−33.0	−0.2
HS 111	1,470	Fragments	Mound			−34.4	−1.5
HS 110	1,480	Fragments	Mound			−35.1	−1.5
HS 109	1,490	Fragments	Mound			−35.4	−1.5
HS 22	1,495	Fragments	Mound	−28.4	−2.0	−32.6	−1.5
HS 42	1,510	Fragments	Mound			−35.6	−1.5
HS 42	1,510	Fragments	Mound	−38.6	2.9		
HS 42	1,510	Fragments	Mound			−35.6	−1.5
HS 28	1,560	Veins	Mound	−1.1	−4.0		
HS 44	1,655	Fragments	Eye	−38.8	−0.3		

source (e.g. Hesse and Harrison 1981; Ussler and Paull 1995; Aloisi et al. 2000; Deyhle and Kopf 2001).

Some of the group II carbonates have elevated $\delta^{18}O$ values reaching 5.8‰. This is too high to be a diagenetic temperature effect, as calcite within 40 m in the borehole have a difference in $\delta^{18}O$ reaching 6.7‰. Calculations of the theoretical fractionation of oxygen isotopes between dissolved carbonate and calcite show that the corresponding difference in temperature is about 24 °C (using the same $\delta^{18}O_{water}$ for both, and the equation of Epstein et al. 1953). This is geologically unrealistic, and suggests the carbonates precipitated from fluids with very different $\delta^{18}O$ signatures. The water temperature at the time of formation is not known (making precise estimates of $\delta^{18}O_{water}$ impossible), but it is reasonable to conclude that the $\delta^{18}O$-enriched carbonates precipitated from a $\delta^{18}O$-enriched fluid. Water released from gas hydrate is a good candidate for this component (e.g. Hesse and Harrison 1981; Ussler and Paull 1995; Martin et al. 1996; Bohrmann et al. 1998; Aloisi et al. 2000; Greinert et al. 2001). This suggests that the Miocene–Pliocene seep development of the complex was associated with gas hydrates. The $\delta^{13}C$ values of these carbonates are more enriched than those of the carbonates deeper in the borehole (< -46‰ compared to > -39‰), pointing towards a biogenic source of methane.

The majority of the carbonates from group II have oxygen isotope ratios in the range −1 to 2.5‰ (Table 1). The average $\delta^{18}O$ between 1,407 and 1,445 m is 0.4‰,

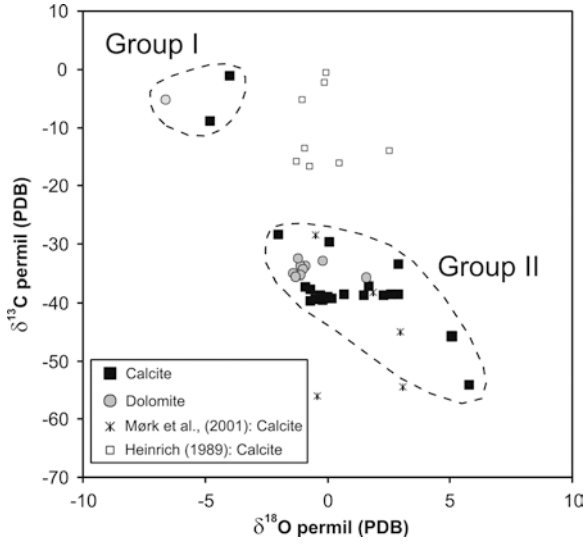

Fig. 7 Stable isotope data of calcite and dolomite from the 1,300–1,700 m interval fall in two distinct groups (*I* and *II*). Calcite isotope data from other cores in the Vøring Basin are shown for reference, with Eocene seep calcite (Mørk et al. 2001), and early diagenetic calcite from organic-rich sequences (Heinrich 1989)

which gives theoretical temperatures of formation in the range 15–19 °C (assuming a $\delta^{18}O_{water}$ between 0 and 1‰, and using the equation of Epstein et al. 1953). This supports the suggestions from the textural relations that aragonite was a precursor to the radial aggregates of

calcite, and that the calcite formed during burial and recrystallization.

Seeps and hydrothermal vent complexes

The seep-carbonate horizons in the Miocene–Eocene–Pliocene strata may have important implications for the hydrogeological system in the Vøring Basin. With the Paleocene–Eocene transition as the timing for initiation of seeps (Fig. 4), we have a documented seep record lasting about 50×10^6 years. We suggest that this seep record is related to the underlying hydrothermal vent complex. The hydrothermal vent complexes in the Vøring Basin were explosive and short-lived events (Jamtveit et al. 2003). Thus, the seep record is not directly related to the thermal anomaly of the system as, for example, in the Guaymas Basin (e.g. Simoneit et al. 1988).

There is one scenario which can explain the presence of seep carbonate above the 6607/12-1 hydrothermal vent complex, with the migration of possibly thermogenic methane and hydrocarbons from deeper levels in the basin. Fluids may migrate through the lower part of the hydrothermal vent complex (i.e. in the conduit zone), similar to fluid seepage through mud volcano conduits during dormant periods (e.g. Higgins and Saunders 1974; Le Pichon et al. 1990; Dia et al. 1999). Some of the methane could be trapped as hydrate below the seafloor. This would imply that hydrothermal vent complexes act as a vertical high-permeability zone during further burial of the basin. Another possibility is that the permeability in the conduit zone is produced by differential compaction of the hydrothermal vent complex, leading to a localized fracture zone. However, the carbonate record in 6607/12-1 shows that seeps formed during or shortly after the hydrothermal vent complex formation, which should not have been the case if it was controlled by later differential compaction.

Conclusions

Petrological and geochemical data from the 6607/12-1 well in the Vøring Basins show that hydrothermal processes and structures may have an important control on the formation of seep deposits. Isotope and petrological data on calcite and dolomite ($\delta^{13}C$ showing methanogenic signatures) show that hydrocarbons migrating through the hydrothermal vent complex during, and shortly after its formation are oxidized by bacteria via sulphate reduction close to the seafloor. A 50×10^6 year record of seep carbonate from the borehole indicates that the hydrothermal vent complex rocks can later act as fluid migration pathways.

Hydrothermal vent complexes may thus be important when considering geological–biological interactions and release of seep-gases to the water column and the atmosphere, as they may act as high-permeability conduits.

Acknowledgments This study was supported by grant 120897 to Jamtveit/Svensen and by the FUNN program (analytical work) from the Norwegian Research Council. We would like to thank TGS-NOPEC for access to seismic data, and Debra Stakes and an anonymous reviewer for constructive comments. This work was motivated by a seismic profile appearing in an article by H. Carstens in GEO (September 2001), showing the position of the 6607/12-1 borehole and the eye structure (described as a buried mud volcano).

References

Adshead JD (1996) Stable isotopes, 14C dating, and geochemical characteristics of carbonate nodules and sediment from an active vent field, northern Juan de Fuca Ridge, northeast Pacific. Chem Geol 129:133–152

Aharon P (1994) Geology and biology of modern and ancient submarine hydrocarbon seeps and vents: an introduction. Geo-Mar Lett 14:69–73

Aiello IW, Garrison RE, Moore JC, Kastner M, Stakes D (2001) Anatomy and origin of carbonate structures in a Miocene cold-seep field. Geology 29:1111–1114

Aloisi G, Pierre C, Rouchy J-M, Foucher J-P, Woodside J, MEDINAUT Scientific Party (2000) Methane-related authigenic carbonates of eastern Mediterranean Sea mud volcanoes and their possible relation to gas hydrate destabilization. Earth Planet Sci Lett 184:321–338

Blunck TD, Blanchet H (1986) 6607/12-1 final report. Elf Aquitane Norge a/s

Blystad P, Brekke H, Færseth RB, Larsen B, Skogseid J, Tørudbakken B (1995) Structural elements of the Norwegian continental shelf. Part II. The Norwegian Sea region. The Norwegian Petroleum Directorate, NPD Bull no 8

Boetius A, Ravenschlag K, Scubert CJ, Rickert D, Widdel F, Gieseke A, Amman R, Jørgensen BB, Witte U, Pfannkuche O (2000) A marine microbial consortium apparently mediating anaerobic oxidation of methane. Nature 407:623–626

Bohrmann G, Greinert J, Suess E, Torres M (1998) Authigenic carbonates from the Cascadia subduction zone and their relation to gas hydrate stability. Geology 26:647–650

Brooks JM, Kennicutt MC, Fay RR, McDonald TJ (1984) Thermogenic gas hydrates in the Gulf of Mexico. Science 225:409–411

Campbell KA, Farmer JD, Des Marais D (2002) Ancient hydrocarbon seeps from the Mesozioc convergent margin of California: carbonate geochemistry, fluids and palaeoenvironments. Geofluids 2:63–94

Cita MB, Woodside JM, Ivanov MK, Kidd RB, Limonov AF, Scientific Party Cruise TTR3—Leg 2 (1995) Fluid venting from a mud volcano in the Mediterranean Ridge Diapiric Belt. Terra Nova 7:453–458

Deyhle A, Kopf A (2001) Deep fluids and ancient pore waters at the backstop: stable isotope systematics (B, C, O) of mud-volcano deposits on the Mediterranean Ridge accretionary wedge. Geology 29:1031–1034

Dia AN, Castrec-Rouelle M, Boulègue J, Comeau P (1999) Trinidad mud volcanoes: where do the expelled fluids come from? Geochim Cosmochim Acta 63:1023–1038

Elvert M, Greinert J, Suess E (2001) Carbon isotopes of biomarkers derived from methane-oxidizing microbes at Hydrate Ridge, Cascadia convergent margin. Geophys Monogr 124:115–129

Epstein S, Buchsbaum R, Lowenstam H, Urey HC (1953) Revised carbonate-water isotopic temperature scale. Geol Soc Am Bull 64:1315–1326

Gaillard C, Rio M, Rolin Y, Roux M (1992) Fossil chemosynthetic communities related to vents or seeps in sedimentary basins: the pseudobioherms of Southwestern France compared to other world examples. Soc Econ Paleontol Mineral 7:451–465

Greinert J, Bohrmann G, Suess E (2001) Gas hydrate-associated carbonates and methane-venting at Hydrate Ridge: classification, distribution, and origin of authigenic lithologies. In: Natural gas hydrates: occurrence, distribution, and detection. Geophys Monogr 124:99–113

Hein JR, O'Neil JR, Jones MG (1979) Origin of authigenic carbonates in sediment from the deep Bering Sea. Sedimentology 26:681–705

Heinrich R (1989) Diagenetic environments of authigenic carbonates and opal-CT crystallization in lower Miocene to upper Oligocene deposits of the Norwegian Sea (ODP Site 643, Leg 104). In: Eldholm O, Thiede J, Taylor E (eds) Proc Ocean Drilling Program, Sci Results 104:233–247

Hesse R, Harrison WE (1981) Gas hydrates (clathrates) causing pore-water freshening and oxygen isotope fractionation in deep-water sedimentary sections of terrigenous continental margins. Earth Planet Sci Lett 55:453–462

Higgins GE, Saunders JB (1974) Mud volcanoes—their nature and origin. Verhandl Naturf Ges Basel 84:101–152

Higgins IJ, Quale JR (1970) Oxygenation of methane by methane-grown *Pseudomonas methanica* and *Methanomonas methanooxidans*. Biochem J 118:201–208

Hinrichs K-U, Hayes JM, Sylva SP, Brewer PG, DeLong EF (1999) Methane-consuming archaebacteria in marine sediments. Nature 398:802–805

Hovland M, Judd A (1988) Seabed pockmarks and seepages: impact on geology, biology and the marine environment. Graham and Trotman, London

Hovland M, Talbot MR, Qvale H, Olaussen S, Aasberg L (1987) Methane-related carbonate cements in pockmarks of the North Sea. J Sediment Petrol 57:881–892

Irwin H, Curtis C, Coleman M (1977) Isotopic evidence for source of diagenetic carbonates formed during burial of organic-rich sediments. Nature 269:209–213

Jakubov AA, Ali-Zade AA, Zeinalov MM (1971) Grayazeve vulkany Azerbaidzhanskoi SSR: Atlas (Mud volcanoes of the Azerbaijan SSR). Azerbaijan Acad Sci, Baku

Jamveit B, Svensen H, Podladchikov JJ, Planke S (2003) Hydrothermal vent complexes associated with sill intrusions in sedimentary basins. Geol Soc Lond Spec Publ (in press)

Kohn MJ, Riciputi LR, Stakes D, Orange DL (1998) Sulfur isotope variability in biogenic pyrite: reflections of heterogeneous bacterial colonization? Am Mineral 83:1454–1468

Kopf A, Behrmann JH (2000). Extrusion dynamics of mud volcanoes on the Mediterranean Ridge accretionary complex. Geol Soc Spec Publ 174:169–204

Le Pichon X, Foucher J-P, Boulègue J, Henry P, Lallemant S, Benedetti M, Avedik F, Mariotti A (1990) Mud volcano field seaward of the Barbados Accretionary Complex: a submersible survey. J Geophys Res 95(B6):8931–8943

Martin JB, Kastner M, Henry P, Le Pichon X, Lallement S (1996) Chemical and isotopic evidence of sources of fluids in a mud volcano field seaward of the Barbados accretionary wedge. J Geophys Res 101:20325–20345

Milkov AV (2000) Worldwide distribution of submarine mud volcanoes and associated gas hydrates. Mar Geol 167:29–42

Mørk MBE, Leith DA, Fanavoll S (2001) Origin of carbonate-cemented beds on the Naglfar Dome, Vøring Basin, Norwegian Sea. Mar Petrol Geol 18:223–234

Paull CK, Chanton JP, Neumann AC, Coston JA, Martens CS (1992) Indicators of methane-derived carbonates and chemosynthetic organic carbon deposits: examples from the Florida escarpment. Palaios 7:361–375

Peckmann J, Reimer A, Luth U, Hansen BT, Heinicke C, Hoefs J, Reitner J (2001) Methane-derived carbonates and authigenic pyrite from the northwestern Black Sea. Mar Geol 177:129–150

Raisewell R (1987) Non-steady state microbiological diagenesis and the origin of concretions and nodular limestones. In: Marshall JD (ed) The diagenesis of sedimentary sequences. Geol Soc Spec Publ 36:41–54

Reeburg WS (1980) Anaerobic methane oxidation: rate depth distribution in Skan Bay sediments. Earth Planet Sci Lett 47:345–352

Ritger S, Carson B, Suess E (1987) Methane-derived authigenic carbonates formed by subduction-induced pore-water expulsion along the Oregon/Washington margin. Geol Soc Am Bull 98:147–156

Roberts HH, Aharon P (1994) Hydrocarbon-derived carbonate buildups of the northern Gulf of Mexico continental slope: a review of submersible investigations. Geo-Mar Lett 14:135–148

Robertson A, Ocean Drilling program Leg 160 Scientific Party (1996) Mud volcanism on the Mediterranean Ridge: initial results of Ocean Drilling Program Leg 160. Geology 24:239–242

Simoneit BRT, Kawka OE, Brault M (1988) Origin of gases and condensates in the Guaymas Basin hydrothermal system (Gulf of California). Chem Geol 71:169–182

Stakes DS, Orange D, Paduan JB, Salamy KA, Mahler N (1999) Cold-seeps and authigenic carbonate formation in Monterey Bay, California. Mar Geol 159:93–109

Suess E, Whiticar MJ (1989) Methane-derived CO_2 in pore fluids expelled from the Oregon subduction zone. Palaeogeogr Palaeoclimatol Palaeoecol 71:119–136

Ussler W, Paull CK (1995) Effects of ion exclusion and isotopic fractionation on pore water geochemistry during gas hydrate formation and decomposition. Geo-Mar Lett 15:37–44

Vinogradov AP, Galimov EM (1970) Carbon isotopes and the origin of petroleum. Geokhimiya 3:275–296

Whiticar MJ, Suess E, Wehner H (1985) Thermogenic hydrocarbons in surface sediments of the Bransfield Strait, Antarctic Peninsula. Nature 314:87–90